APPLIED PHYSICS LETTERS

Mechanism of droplet-formation in a supersonic microfluidic spray device

T. Kartanas,[1] Z. Toprakcioglu,[1] T. A. Hakala,[1] A. Levin,[1] T. W. Herling,[1] R. Daly,[2] J. Charmet,[3] and T. P. J. Knowles[1,4,a)]

[1)]*Department of Chemistry, University of Cambridge, Lensfield Road, Cambridge CB2 1EW, United Kingdom.*

[2)]*Department of Engineering, University of Cambridge, 17 Charles Babbage Road, Cambridge CB3 0FS, United Kingdom.*

[3)]*Institute of Digital Healthcare, WMG, University of Warwick, Coventry CV4 7AL, United Kingdom.*

[4)]*Cavendish Laboratory, University of Cambridge, Cambridge CB3 1HE, United Kingdom.*

(Dated: 22 March 2020)

Spray drying is an approach employed in automotive, food and pharmaceutical industries as a robust and cost efficient liquid atomisation technique offering direct control over droplet dimensions. The majority of commercially available spray nozzles are designed for large throughput spray drying applications or uniform surface coating, but microfluidic nebulisers have recently been developed as a small scale alternative. Here, we explore the physical parameters that define droplet size and formation under supersonic flow conditions commonly found in microfluidic spray drying systems. We examined the spray nozzle operation using high speed imaging and laser scattering measurements, which allowed us to describe the spray regimes and droplet size distributions. It was determined that by using this spray nozzle device, droplets with diameters of 4-8 μm could be generated. Moreover, we show that the supersonic de Laval nozzle model can be used to predict the average droplet size. Our approach can be used as a platform for interfacing fluid microprocessing with gas phase detection and characterisation.

Liquid atomisation is a key approach for material processing with a wide range of applications in the pharmaceutical, food, chemical, electronic and automotive industries.[1–7] Common routes for liquid droplet generation involve aerosol spraying,[8] inkjet printing[9] and electrospraying.[10] However, these techniques vary both in material compatibility and in droplet monodispersity. Currently, aerosol spraying is by far the most flexible and relatively well understood process.[8,11,12] Typical commercially available aerosol spray nozzles are designed to work at large throughputs and can be used to generate droplets with diameters ranging between 3 μm and 100 μm,[13,14] depending on the nozzle dimension.[15]

In recent years, novel types of microfluidic pneumatic spray nozzles have gained interest due to low dead-volume and the ease at which devices can be fabricated using conventional rapid prototyping soft-lithography approaches.[16–19] In contrast to industrial-scale nozzles, microfluidic spray devices can produce droplets with diameters ranging from 10 μm down to 300 nm, which is smaller than their characteristic orifice sizes of 50-100 μm.[20] Droplets of reduced size evaporate quicker due to the increased surface to volume ratio and, therefore, such devices have been used for applications, requiring quick evaporation, such as amorphous nanoparticle formation,[20–22] femtosecond X-ray crystallography,[23] mass spectrometry,[24] biosensing[25–27] as well as artifact-free sample preparation for surface probe microscopy.[28] However, the physical parameters that define droplet size and formation under supersonic flow conditions have not yet been characterised in detail.

In this paper, we firstly describe the fabrication and operation of a microfluidic spray nozzle, featuring a non-planar or 3-dimentional (3D) non-wetting liquid junction depicted in Fig. 1(a). Microfluidic spray devices usually combine a liquid channel with pressurised gas channels (air or nitrogen) with typical relative pressures between 0.1 bar and 3 bar. At low pressures, the spray devices have been shown to operate in a jetting regime to create monodisperse droplet distributions,[23,29] where the droplet breakup is induced by the Rayleigh-Taylor instability.[30] Intuitively, the resultant drop size reduces when higher pressures are applied, which results in the increased gas flow rate. However, at a certain pressure threshold, the flow through the gas channel is choked as the gas velocity approaches sonic speeds at the nozzle orifice.[11] In this study, we describe how aqueous airborne micron-sized droplets are generated within a supersonic microfluidic spray device and how the applied gas pressure influences the corresponding droplet size. We use the de Laval nozzle choked flow adiabatic expansion model (Fig. 1b) to predict the gas speeds and the average droplet size.

The microfluidic devices were fabricated using a standard soft-lithographic approach[17] and then cast using polydimethylsiloxane (PDMS). The device used had non-planar (3D) geometry, and therefore the channels are completely surrounded by PDMS. This is a hydrophobic material, with a water contact angle of >100°.[31] A hydrophobic material is needed for effective device operation, as the water will not wet and adsorb onto the nozzle and will instead break-off resulting in the formation of a spray. For the purpose of our study we found that the contact angle of pure PDMS was high enough to ensure reproducible and robust device operation and no surface modification was thus needed. In order to make the 3D junction, a two step photolithographic process was used. A 25 μm tall structure was first fabricated using the mask shown in Fig. 2(a). These structures were then aligned with 50 μm tall channels fabricated from the mask shown in Fig. 2(b). The design of the resultant master is schematically depicted in Fig. 2(c). The device contains one inlet for the gas phase and one inlet for liquid phase, as shown

a)Electronic mail: tpjk2@cam.ac.uk

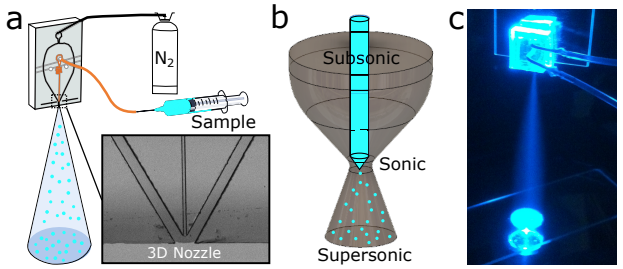

FIG. 1. Supersonic microfluidic single junction spray nozzle. (a) Schematic representation of the 3 dimensional (3D) nozzle atomising liquid with a supersonic pressurised gas flow through a constriction. Inset: Optical micrograph of the device at the 3D nozzle area. (b) Schematic representation of the de Laval converging-diverging nozzle model. The gas flow through the device can be explained using this model. Initially subsonic gas flow upstream is choked at the narrowest device part (throat) and then is accelerated to supersonic speeds at the nozzle outlet. (c) Image of the spray nozzle device in action. A fluorescent dye was added to the aqueous phase in order to monitor the spray in real-time.

schematically in Fig. 1(a). The liquid channel cross-section is 25×20 μm^2 and the gas channel assembly is 100×100 μm^2. One of the key integral parts of the device is the three dimensional nozzle, (optical micrograph in Fig. 1(a)). This geometry is obtained by plasma bonding two PDMS complementary replicas with channels on each side,[25,32] the process of which is shown in Fig. 2(d-e). The two sides of the device were aligned with respect to each another using a thin water lubrication layer. This geometry allows for the liquid to be completely surrounded by the gas flow, thus promoting the fluid transportation through the nozzle in the form of a jet, without PDMS surface wetting. It was found that the larger the liquid channel, the higher the probability of the device to malfunction. A larger liquid channel allows for more water to collect at the nozzle to the point where the drag force is not high enough to form a liquid jet and subsequently water droplets drip rather than being sprayed from the device, leading to the generation of massive (>50 μm) droplets. Moreover, an increase or decrease in air channel dimension did not significantly change device operation or droplet sizes and their respective distribution. The device gas inlet was connected to a compressed nitrogen cylinder and the liquid phase was controlled using a syringe pump (Harvard Apparatus PHD2000). Precision glass syringes (Hamilton gastight 1800 series) were connected to the device via polyethylene tubing (Smiths Medical, 800/100/120).

Aqueous droplets were produced in a supersonic nitrogen flow using a microfluidic spray nozzle. Due to the resemblance of the design geometry to the de Laval converging-diverging nozzle, such a system was used to model flow and droplet generation. To visualise the drop formation at the nozzle, the use of a high-speed camera (V310, Phantom, USA), operated at 25,000 frames per second and 1 μs exposure time was employed. Droplet generation through the spray nozzle can be seen in Figure 3. It was observed that the spray operates in a pulsating mode: first, a drop of 30-50 μm in diameter builds up at the gas stagnation point until it is large enough

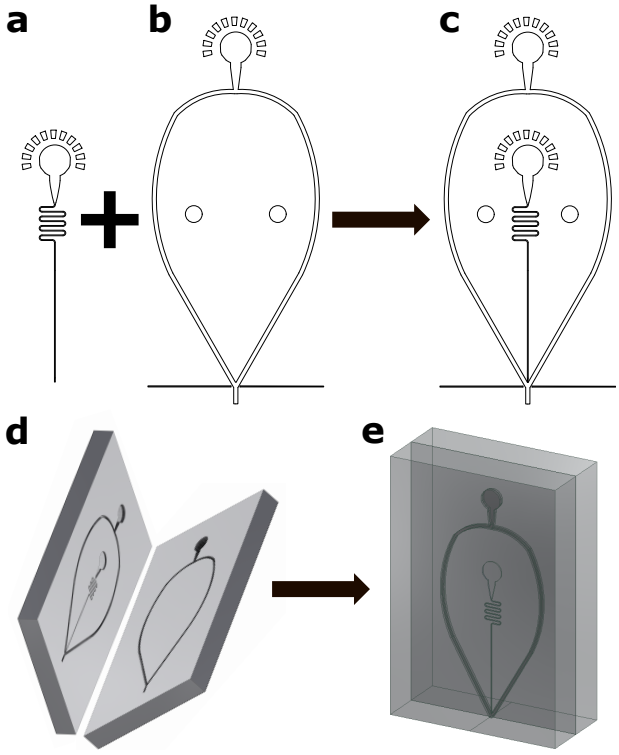

FIG. 2. Supersonic microfluidic spray nozzle. (a-c) Mask design and spray nozzle components. (a) 25 μm high liquid channel. (b) 50 μm high gas channel and (c) their combination using a two-step lithography process. (d-e) Assembly of the two PDMS layers via plasma bonding. The PDMS pieces in (d) come from the two respective masters. The two-layer master (c) and the single layer master (b). A thin layer of water was added between the two PDMS layers, before they were carefully aligned with respect to one another. The PDMS slabs were then left to bond, resulting in the 3D device (e).

and the drag force due to the sonic gas flow is high enough to form a liquid jet (see Figure 3a). Using high speed imaging, we could also estimate that the liquid jet has an average diameter of $d_{jet} \approx 10$ μm. A series of images were used to observe the device operation and it was found that this droplet break-up process is highly reproducible with a frequency of 700 Hz at a flow rate Q = 100 μLh^{-1} and the pressure 2 bar.

To observe the jet-to-droplet transition during jetting events, we focused the camera just below the nozzle orifice. The pressure at the gas inlet was varied between 0.4 bar and 2 bar and the jet break-up was observed as shown in Fig. 3b. Qualitatively, we could observe two distinct spraying regime, where a transition from a few large droplets at a pressure of 0.4 bar to multiple, smaller droplets occurs at higher pressures. The change in nozzle operation could thus clearly be identified from the change in droplet distributions between a pressure of 0.8 and 1.2 bar. Finally, we focused the imaging area 3 cm below the nozzle orifice to estimate the droplet speed upon impact on a target surface area. This was measured as $v_d \approx 20$ ms^{-1} using the high speed images and averaging over multiple frames.

To explain the spray device operation, the choked flow de Laval nozzle model[11] was applied. The flow of gas at an up-

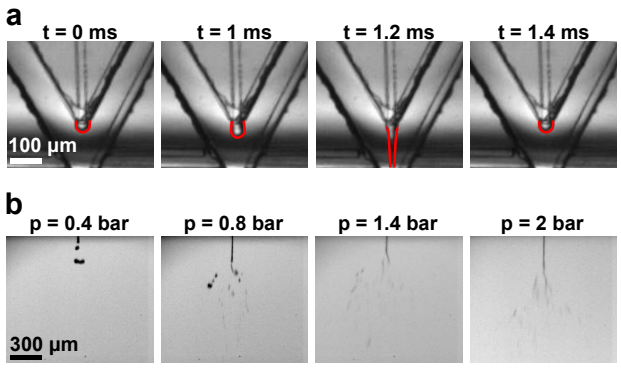

FIG. 3. Nozzle operation for water solution flowing at 100 μLh^{-1}. (a) Nitrogen pressure of $\Delta p = 2$ *bar* is applied and the device is operating in a dripping regime: a droplet at the liquid outlet is formed and increases in size until it is elongated and ejected through the device orifice with a frequency of ≈700 Hz . (b) The generated jet breaks into droplets outside the device due to the instabilities caused by high shear forces. The spray is studied as a function of the gas pressure. At low pressures, a small number of large droplets is generated, but droplet size qualitatively decreases with increasing gas pressure.

stream stagnant pressure, p_0, guided through a narrow constriction (the microfluidic channel in our case) into a wide exit at a pressure, p_e, depends on the pressure difference $\Delta p = p_0 - p_e$. At a low pressure difference, Δp, the flow can be approximated as laminar, however, as Δp increases, the gas velocity increases at the nozzle throat until it reaches the local speed of sound. At that point, the flow is choked due to the sonic shocks which results in the increased gas flow friction.[11] Additional increase of an upstream pressure, p_0, results in an increased flowing gas density at the throat, but the speed is still confined to the sonic limit.

The critical pressure difference for the choked flow to occur is when p_e is lower than the critical pressure p_c given by

$$p_c = p_u \left(\frac{2}{\gamma+1} \right)^{\frac{\gamma}{\gamma-1}} \tag{1}$$

where $\gamma = c_p/c_v$ is the ratio of gas specific heat capacities at constant pressure and volume.[33] For nitrogen (also air), $\gamma = 1.4$, giving $p_c = 0.528 p_0$; hence, for a spray nozzle operating under normal atmospheric conditions, p_e=p_a. Choked flow will thus occur if $p_0 > 1.9$ bar or $\Delta p > 0.9$ bar. In the described system, the nozzle was operated at Δp between 2 – 3 bar to achieve stable spraying. Therefore, at our typical spray nozzle operation conditions, the gas flow is choked.

The sonic gas flow experiences a sudden divergent expansion just outside the nozzle throat and, thus, can achieve supersonic speeds in the vicinity of the nozzle orifice. The linear velocity, v_e, of gas exiting the nozzle under the assumption of an ideal adiabatic gas expansion behaviour[34] is:

$$v_e = \sqrt{\frac{RT}{M} \cdot \frac{2\gamma}{\gamma-1} \cdot \left[1 - \left(\frac{p_e}{p_u} \right)^{(\gamma-1)/\gamma} \right]} \tag{2}$$

TABLE I. . Drop size prediction as a function of applied pressure difference.

Pressure Δp / bar	Velocity v_e / m/s	Drop diameter d_d / μm
1.5	370	7.5
2	400	6.4
2.5	430	5.8
3	440	5.3

where v_e is the gas exit velocity, R is the universal gas constant and M is the gas molar mass. Under the usual spray operating condition ($\Delta p = 3$ bar), the maximum gas exit speed was estimated to be $v_{3bar} = 450\text{ms}^{-1}$. As soon as the supersonic gas jet emerges from the nozzle, imparts a destabilising high shear force to the emerging liquid jet, driving a break up into droplets.

To explain the droplet formation, we consider the shear stress caused by the large speed difference between the emerging gas and the formed liquid droplets $\Delta v = v_e - v_d \approx v_e$. The shear forces destabilise the liquid-gas interface forming surface waves - the Rayleigh-Taylor type of instability - eventually leading to the jet breakup.[30] We estimate the size distribution of the droplets by considering the balance between supersonic aerodynamic shear stress and the liquid-gas interfacial surface tension

$$\frac{1}{2} C_d \rho_g (v_e - v_d)^2 = \frac{2\gamma}{R_d} \tag{3}$$

where ρ_g and v_e are the gas density and speed, R_d and v_d are the generated drop radius and speed, γ is the surface tension, C_d is the coefficient of drag of around 0.47 for a smooth sphere at high Reynolds numbers.[35] By considering that the droplets are much slower than the jet $v_d \ll v_e$, the diameter of the generated droplets can be approximated by

$$d_d = \frac{8\gamma}{C_d \rho_g v_e^2} \tag{4}$$

At gas pressures between 1.5-3 bar we predict droplet diameters to be roughly between 5-8 μm as shown in Table I.

To validate the spray nozzle operation mechanism and predicted values, a laser scattering system (Spraytec, Malvern, UK) was used to measure the generated droplet sizes and mist properties. The nozzle was held 2 cm above the laser beam and the measurement integration time was set to 10 s to accumulate a sufficient signal. First, we investigated the generated drop size distribution at a pressure difference of $\Delta p = 3$ bar and a flow rate 200 μL h^{-1}. We observed that the spray nozzle produced a uni-modal distribution, with a span ranging from 3.75 to 7.36 μm (10-90%) and with a median value of 5.3 μm. This data is shown in Fig. 4a. It should be mentioned that as expected, droplet sizes could be varied by altering the spraying conditions, however, their distribution remained unimodal.

In order to observe the effect of pressure on the generated droplet size, the liquid flow was fixed at 200 μLh^{-1}, while the gas pressure, Δp, was varied between 1.5 bar and 3 bar. As expected, the droplet diameter decreased for increasing gas

pressures from about 8 μm to 5 μm as shown in Fig. 4b. This result is in close agreement with the mean droplet size prediction in Table I, which is also plotted as the red line in Fig. 4b. We could not measure the drop size at pressures below 1.5 bar due to the low scattering signal of smaller number of large droplets.

Next, the pressure was fixed to 3 bar, and the nozzle operation with varying liquid flows between (200 - 400) μL h^{-1} was investigated. We observed a slight increase in droplet diameter from 5.3 μm to 6.3 μm, which is illustrated in Fig. 4c. This increase in the average drop size correlates well with the data gained from the high-speed imaging experiments. By varying the liquid flow rate, we mainly influence the frequency of droplet production rather than controlling the size of the droplets. Of course, there should be a limit where the nozzle will start to operate in the jetting regime, which may affect the droplet size distribution.

Finally, we investigated the device-to-device variation and reproducibility at Δp = 3 bar and Q = 200 μL h^{-1}. Three different well-operating nozzles were tested and it was confirmed that the spray nozzles yield reproducible droplet size distributions. The average median droplet size was found to be 5.3 μm, and even though the spread of droplet size is large, all three measurements yield similar results indicating that device reproducibility is high even if controlling the exact droplet size at such small length-scales may be challenging. This is depicted in Fig. 4d.

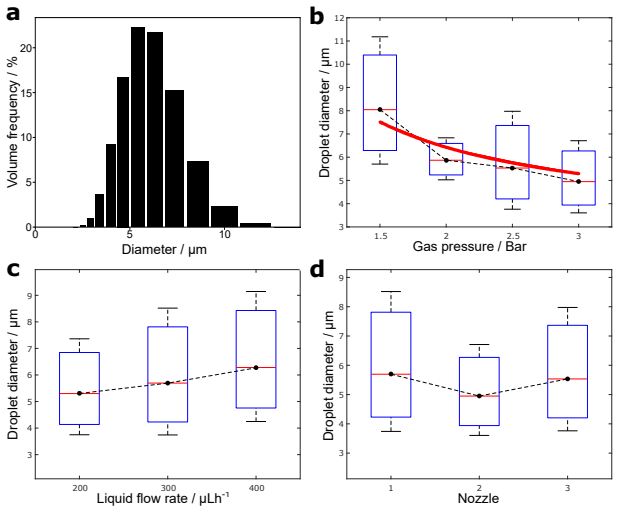

FIG. 4. Droplet size distributions measured 2 cm away from the nozzle orifice. (a) The measured size distribution of droplets at Δp=3 bar and Q=200μL h^{-1}. (b) Droplet size variation as a function of gas pressure shows an expected generated droplet size decrease. The red solid line represents the expected droplet size while the dashed line represents the actual measurements. (c) Droplet diameter increases slowly with increasing liquid flow rate indicating a bias towards larger generated drop sizes. (d) Nozzle-to-nozzle variation is tested at Δp=3 bar and Q=200μL h^{-1} giving an average droplet diameter of 5.3 μm.

Traditional liquid atomisation methods are difficult to engineer and prototype. In this paper, we present a simple strategy to fabricate a microfluidic version of an aerosol spray.

We investigated the physical principles underlying the operation of such a device and have found that there exists a fundamental change in the spray behaviour at pressure difference of about 1 bar. We have used the de Laval converging-diverging nozzle to model the gas flow in the device, which allowed us to predict supersonic gas flow at the nozzle exit. The supersonic flow exerts high shear forces on the emerging droplets, thus atomising the liquid into drops of approximately 5 μm in diameter. We have confirmed our predictions by measuring droplet size distributions and variations as a function of liquid flow rate and device pressure. This droplet generation method described in the present paper provides a platform for material drying and deposition in the gas phase by microfluidic spraying. Due to the high interest in spray-drying and dry mass detection, we believe that this strategy could be further employed in the context of analytical chemistry, where a small amount of surface spray drying is required, for example IR spectroscopy or scanning electron microscopy.

The research leading to these results has received funding from the European Research Council under the European Union's Seventh Framework Programme (FP7/2007-2013) through the ERC grant PhysProt (agreement no. 337969), the BBSRC, the Frances and Augustus Newman Foundation, the Monash Warwick Alliance, the Oppenheimer Early Career Fellowship and the Cambridge Centre for Misfolding Diseases.

[1] J. B. Schlenoff, S. T. Dubas, and T. Farhat, "Sprayed polyelectrolyte multilayers," Langmuir **16**, 9968–9969 (2000).
[2] K. C. Krogman, J. L. Lowery, N. S. Zacharia, G. C. Rutledge, and P. T. Hammond, "Spraying asymmetry into functional membranes layer-by-layer," Nature materials **8**, 512 (2009).
[3] H. Tang, S. Ji, L. Gong, H. Guo, and G. Zhang, "Tubular ceramic-based multilayer separation membranes using spray layer-by-layer assembly," Polymer Chemistry **4**, 5621–5628 (2013).
[4] T. Martini, C. Chubilleau, O. Poncelet, A. Ricaud, A. Blayo, C. Martin, and K. Tarasov, "Spray and inkjet fabrication of cu2znsns4 thin films using nanoparticles derived from a continuous-flow microwave-assisted synthesis," Solar Energy Materials and Solar Cells **144**, 657–663 (2016).
[5] E. A. Redman, N. G. Batz, J. S. Mellors, and J. M. Ramsey, "Integrated microfluidic capillary electrophoresis-electrospray ionization devices with online ms detection for the separation and characterization of intact monoclonal antibody variants," Analytical chemistry **87**, 2264–2272 (2015).
[6] C. A. Smith, X. Li, T. H. Mize, T. D. Sharpe, E. I. Graziani, C. Abell, and W. T. Huck, "Sensitive, high throughput detection of proteins in individual, surfactant-stabilized picoliter droplets using nanoelectrospray ionization mass spectrometry," Analytical chemistry **85**, 3812–3816 (2013).
[7] K. Higashi, K. Uchida, A. Hotta, K. Hishida, and N. Miki, "Micropatterning of silica nanoparticles by electrospray deposition through a stencil mask," Journal of laboratory automation **19**, 75–81 (2014).
[8] P. Marmottant and E. Villermaux, "On spray formation," Journal of fluid mechanics **498**, 73–111 (2004).
[9] M. Singh, H. M. Haverinen, P. Dhagat, and G. E. Jabbour, "Inkjet printing—process and its applications," Advanced materials **22**, 673–685 (2010).
[10] J. B. Fenn, M. Mann, C. K. Meng, S. F. Wong, and C. M. Whitehouse, "Electrospray ionization–principles and practice," Mass Spectrometry Reviews **9**, 37–70 (1990).
[11] P. D. Hede, P. Bach, and A. D. Jensen, "Two-fluid spray atomisation and pneumatic nozzles for fluid bed coating/agglomeration purposes: A review," Chemical Engineering Science **63**, 3821–3842 (2008).
[12] Q. Ye, B. Shen, O. Tiedje, T. Bauernhansl, and J. Domnick, "Numerical and experimental study of spray coating using air-assisted high-pressure atomizers," Atomization and Sprays **25** (2015).

[13]"Okawara mfg co., ltd." http://www.oc-sd.co.jp/english/atomization.html, accessed: 2018-08-21.
[14]C. Arpagaus, "A novel laboratory-scale spray dryer to produce nanoparticles," Drying Technology **30**, 1113–1121 (2012).
[15]K. Cal and K. Sollohub, "Spray drying technique. i: Hardware and process parameters," Journal of pharmaceutical sciences **99**, 575–586 (2010).
[16]J. C. McDonald and G. M. Whitesides, "Poly (dimethylsiloxane) as a material for fabricating microfluidic devices," Accounts of chemical research **35**, 491–499 (2002).
[17]P. K. Challa, T. Kartanas, J. Charmet, and T. P. Knowles, "Microfluidic devices fabricated using fast wafer-scale led-lithography patterning," Biomicrofluidics **11**, 014113 (2017).
[18]Z. Toprakcioglu, P. K. Challa, A. Levin, and T. P. J. Knowles, "Observation of molecular self-assembly events in massively parallel microdroplet arrays," Lab on a Chip **18**, 3303–3309 (2018).
[19]X. Liu, Z. Toprakcioglu, A. J. Dear, A. Levin, F. S. Ruggeri, C. G. Taylor, M. Hu, J. R. Kumita, M. Andreasen, C. M. Dobson, U. Shimanovich, and T. P. J. Knowles, "Fabrication and Characterization of Reconstituted Silk Microgels for the Storage and Release of Small Molecules," Macromolecular Rapid Communications **40**, 1800898 (2019).
[20]E. Amstad, M. Gopinadhan, C. Holtze, C. O. Osuji, M. P. Brenner, F. Spaepen, and D. A. Weitz, "Production of amorphous nanoparticles by supersonic spray-drying with a microfluidic nebulator," Science **349**, 956–960 (2015).
[21]J. Thiele, M. Windbergs, A. R. Abate, M. Trebbin, H. C. Shum, S. Förster, and D. A. Weitz, "Early development drug formulation on a chip: Fabrication of nanoparticles using a microfluidic spray dryer," Lab on a Chip **11**, 2362–2368 (2011).
[22]Z. Toprakcioglu, P. K. Challa, D. B. Morse, and T. Knowles, "Attolitre protein nanogels from droplet nanofluidics for intracellular delivery," **6**, 1–8 (2020).
[23]M. Trebbin, K. Krüger, D. DePonte, S. V. Roth, H. N. Chapman, and S. Förster, "Microfluidic liquid jet system with compatibility for atmospheric and high-vacuum conditions," Lab on a Chip **14**, 1733–1745 (2014).
[24]C. Yu, X. Qian, Y. Chen, Q. Yu, K. Ni, and X. Wang, "Three-dimensional electro-sonic flow focusing ionization microfluidic chip for mass spectrometry," Micromachines **6**, 1890–1902 (2015).
[25]T. Kartanas, V. Ostanin, P. K. Challa, R. Daly, J. Charmet, and T. P. Knowles, "Enhanced quality factor label-free biosensing with microcantilevers integrated into microfluidic systems," Analytical chemistry **89**, 11929–11936 (2017).
[26]T. Müller, D. White, and T. Knowles, "Dry-mass sensing for microfluidics," Applied Physics Letters **105**, 214101 (2014).
[27]Z. Toprakcioglu, P. Challa, C. Xu, and T. P. J. Knowles, "Label-Free Analysis of Protein Aggregation and Phase Behavior," ACS Nano **13**, 13940–13948 (2019).
[28]F. S. Ruggeri, J. Charmet, T. Kartanas, Q. Peter, S. Chia, J. Habchi, C. M. Dobson, M. Vendruscolo, and T. P. Knowles, "Microfluidic deposition for resolving single-molecule protein architecture and heterogeneity," Nature Communications **9**, 3890 (2018).
[29]A. M. Gañán-Calvo, "Generation of steady liquid microthreads and micron-sized monodisperse sprays in gas streams," Physical Review Letters **80**, 285 (1998).
[30]L. Rayleigh, "On the stability, or instability, of certain fluid motions," Proceedings of the London Mathematical Society **1**, 57–72 (1879).
[31]T. Trantidou, Y. Elani, E. Parsons, and O. Ces, "Hydrophilic surface modification of pdms for droplet microfluidics using a simple, quick, and robust method via pva deposition," Microsystems and Nanoengineering **3**, 16091 (2017).
[32]Z. Toprakcioglu, A. Levin, and T. P. J. Knowles, "Hierarchical Biomolecular Emulsions Using 3-D Microfluidics with Uniform Surface Chemistry," Biomacromolecules **18**, 3642–3651 (2017).
[33]M. Potter, D. Wiggert, and B. Ramadan, *Mechanics of Fluids* (2010).
[34]P. Biswas, C. Plagan, and C. Plagan, "High-Velocity Inertial Impactors," Environmental Science and Technology **18**, 611–616 (1984).
[35]J. C. Lasheras and E. J. Hopfinger, "Liquid Jet Instability and Atomization in a Coaxial Gas Stream," Annual Review of Fluid Mechanics **32**, 275–308 (2000).